Progress In Electromagnetics Research, PIER 69, 305–322, 2007

EFFICIENT NUMERICAL APPROACH TO ELECTROMAGNETIC SCATTERING FROM THREE-DIMENSIONAL PERIODIC ARRAY OF DIELECTRIC SPHERES USING SEQUENTIAL ACCUMULATION

A. Matsushima, Y. Momoka, M. Ohtsu, and Y. Okuno

Graduate School of Science and Technology
Kumamoto University
2-39-1 Kurokami, Kumamoto, 860-8555 Japan

Abstract—An effective numerical solution is presented for the plane wave scattering by multilayered periodic arrays of dielectric spheres. The treated structure is a fundamental model of photonic crystals having three-dimensional periodicity. The problem is analyzed by the mode matching method, where the electromagnetic fields in the air and dielectric regions are approximated by using the Floquet harmonics and vector spherical wave functions, respectively. They are matched on the junction surfaces in the least squares sense. Introduction of sequential accumulation in the process of QR decomposition reduces the computation time from $O(Q^3)$ to $O(Q^1)$ and the memory requirement from $O(Q^2)$ to $O(Q^1)$, with Q being a number of sphere layers. Numerical results are given for CPU time, speed of convergence, and some band gap characteristics.

1. INTRODUCTION

Much attention has been attracted for electromagnetic scattering from arrays composed of periodic dielectric bodies [1–4], since they are important materials as fundamental photonic crystals [5–7]. Such structures have properties of electromagnetic or optical band gaps, and are frequently used to design interesting devices [8, 9] accompanied with the development of manufacturing technology. Nevertheless, we have small number of reports concerning accurate numerical treatment on three-dimensional structures. This is because the boundary value problems for vector fields are rather complicated. The patch-dipole current model was applied to two dimensionally periodic spherical

array and its numerical error was discussed [10], but we cannot say that the investigation on physical properties is sufficient.

In view of this, the present paper proposes an efficient numerical technique and applies it to plane wave scattering from a three-dimensional periodic array of dielectric spheres. The method is based on the modal expansion of electromagnetic field, which is known as a mode matching method [11] a least squares boundary residual method [12], or an improved point matching method [13]. The electromagnetic fields in the air and dielectric regions are approximated by using the Floquet harmonics and vector spherical wave functions, respectively. They are matched on the junction surfaces in the least squares sense. Recently the present authors extended the range of applicability of this method by combining up- and down-going modal functions to describe the field, which is effective especially for gratings with deep grooves [14]. Special emphasis in the present paper is placed on the introduction of the sequential accumulation [15] in the process of QR decomposition [16] of matrices. This can reduce the computation time from $O(Q^3)$ to $O(Q^1)$ and the memory requirement from $O(Q^2)$ to $O(Q^1)$, where Q is a number of sphere layers in the propagation direction. Numerical results will be given for discussion from the mathematical and physical points of view, i.e., CPU time, speed of convergence, and some band gap characteristics.

2. STATEMENT OF THE PROBLEM

As shown in Fig. 1(a), the dielectric spheres, having the radius a and the relative permittivity ε_{r}, are arranged with the period d in the directions of each axis. The number of spheres is infinity along the x and y axes, and the number of layers is Q. The plane which includes the center of spheres in the q-th layer is $z = z_q = (q-1)d$.

The incident angles θ^{i} and ϕ^{i} are defined in Fig. 1(b). Without loss of generality, we can restrict them to $0 \le \theta^{\mathrm{i}} < \pi/2$ and $0 \le \phi^{\mathrm{i}} \le \pi/4$. The periodicity allows us to consider only over the unit cell $|x|, |y| < d/2$. The time factor $\mathrm{e}^{j\omega t}$ will be omitted throughout.

3. APPROXIMATE WAVE FUNCTIONS

3.1. Semi-Infinite Spaces

The wave vector of the incident field is $\boldsymbol{k}_{00}^{(+)} = k_0(\sin\theta^{\mathrm{i}}\cos\phi^{\mathrm{i}}\,\boldsymbol{i}_x + \sin\theta^{\mathrm{i}}\sin\phi^{\mathrm{i}}\,\boldsymbol{i}_y + \cos\theta^{\mathrm{i}}\,\boldsymbol{i}_z)$, where $k_0 = \omega\sqrt{\varepsilon_0\mu_0} = 2\pi/\lambda$ is a wavenumber in the air, and the symbol $\boldsymbol{i}_u$ $(u = x, y, z)$ is a unit vector in the u

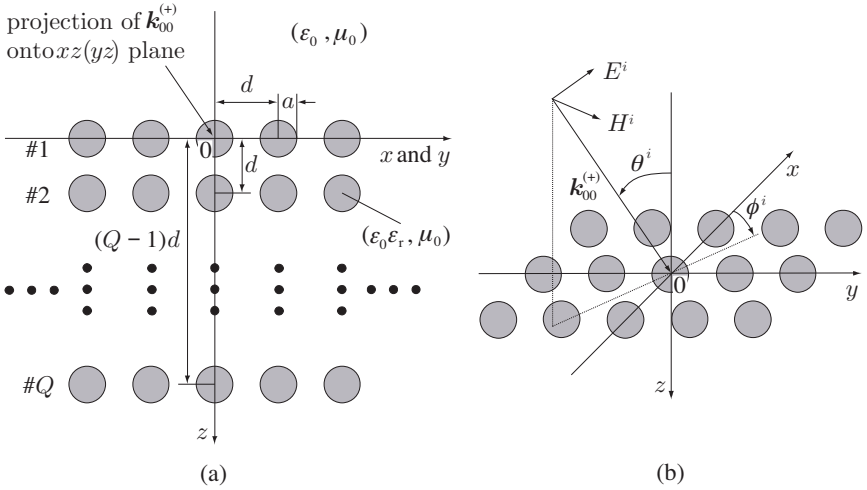

Figure 1. Geometry of the problem. (a) Array of dielectric spheres. (b)Incident plane wave.

direction. This yields the wave vector of the mn-th mode

$$\boldsymbol{k}_{mn}^{(\pm)} = \alpha_m \boldsymbol{i}_x + \beta_n \boldsymbol{i}_y \pm \gamma_{mn} \boldsymbol{i}_z \tag{1}$$

where

$$\begin{cases} \alpha_m = k_0 \sin\theta^{\mathrm{i}} \cos\phi^{\mathrm{i}} + 2m\pi/d, \quad \beta_n = k_0 \sin\theta^{\mathrm{i}} \sin\phi^{\mathrm{i}} + 2n\pi/d \\ \gamma_{mn} = (k_0^2 - \alpha_m^2 - \beta_n^2)^{1/2} \quad (\mathrm{Im}\ \gamma_{mn} \le 0) \end{cases} \tag{2}$$

The upper and lower signs in Eq. (1) go together, which denote the direction of propagation or attenuation. Since the field of the mn-th mode is normal to $\boldsymbol{k}_{mn}^{(\pm)}$, we can introduce the normalized orientation vectors

$$\boldsymbol{e}_{p,mn}^{(\pm)} = \begin{cases} (\boldsymbol{k}_{mn}^{(\pm)} \times \boldsymbol{i}_z)/|\boldsymbol{k}_{mn}^{(\pm)} \times \boldsymbol{i}_z| & (p=1;\ \text{TE-mode}) \\ (\boldsymbol{e}_{1,mn}^{(\pm)} \times \boldsymbol{k}_{mn}^{(\pm)})/|\boldsymbol{e}_{1,mn}^{(\pm)} \times \boldsymbol{k}_{mn}^{(\pm)}| & (p=2;\ \text{TM-mode}) \end{cases} \tag{3}$$

$$\boldsymbol{h}_{p,mn}^{(\pm)} = (\boldsymbol{k}_{mn}^{(\pm)}/k_0) \times \boldsymbol{e}_{p,mn}^{(\pm)} \tag{4}$$

Equations (3) and (4) tell us that the vectors $\boldsymbol{e}_{1,mn}^{(\pm)}$ (TE) and $\boldsymbol{h}_{2,mn}^{(\pm)}$ (TM) are both normal to $\boldsymbol{i}_z$.

The above preparation enables us to write the wave functions in both half spaces. In the air region $z < -d/2$, the incident field is

expressed as

$$\begin{bmatrix} \boldsymbol{E}^{\mathrm{i}} \\ \zeta_0 \boldsymbol{H}^{\mathrm{i}} \end{bmatrix}(P) = \begin{bmatrix} \boldsymbol{e}_{1,00}^{(+)} & \boldsymbol{e}_{2,00}^{(+)} \\ \boldsymbol{h}_{1,00}^{(+)} & \boldsymbol{h}_{2,00}^{(+)} \end{bmatrix} \begin{bmatrix} \cos\delta \\ \sin\delta \end{bmatrix} f_{00}^{(+)}(\boldsymbol{P} + \boldsymbol{i}_z d/2) \tag{5}$$

where $\boldsymbol{P} = x\boldsymbol{i}_x + y\boldsymbol{i}_y + z\boldsymbol{i}_z$ is a position vector of an observation point P, $\zeta_0 = \sqrt{\mu_0/\varepsilon_0}$ is the wave impedance in the air, and the modal function

$$f_{mn}^{(\pm)}(\boldsymbol{P}) = \exp[-j\boldsymbol{k}_{mn}^{(\pm)} \cdot \boldsymbol{P}] \tag{6}$$

is a solution of the Helmholtz equation based on the method of separation of variables. The polarization angles $\delta = 0$ and $\pi/2$ correspond to the TE- and TM-modes, respectively.

We can write the approximate wave function in the transmission region $z > (Q - 1/2)d$ as

$$\begin{bmatrix} \boldsymbol{E}_N \\ \zeta_0 \boldsymbol{H}_N \end{bmatrix}(P) = \sum_{p=1}^{2} \sum_{m=-N}^{N} \sum_{n=-N}^{N} A_{pmn,N} \begin{bmatrix} \boldsymbol{e}_{pmn}^{(+)} \\ \boldsymbol{h}_{pmn}^{(+)} \end{bmatrix} f_{mn}^{(+)}(\boldsymbol{P} - \boldsymbol{i}_z(Q-1/2)d) \tag{7}$$

where N is a number of truncation. A similar manner yields the approximate wave function in the reflection region $z < -d/2$ as

$$\begin{bmatrix} \boldsymbol{E}_N \\ \zeta_0 \boldsymbol{H}_N \end{bmatrix}(P) = \sum_{p=1}^{2} \sum_{m=-N}^{N} \sum_{n=-N}^{N} B_{pmn,N} \begin{bmatrix} \boldsymbol{e}_{pmn}^{(-)} \\ \boldsymbol{h}_{pmn}^{(-)} \end{bmatrix} f_{mn}^{(-)}(\boldsymbol{P} + \boldsymbol{i}_z d/2) \tag{8}$$

Equations (7) and (8) include $4(2N + 1)^2$ unknown expansion coefficients $A_{pmn,N}$ and $B_{pmn,N}$, which depend on the number N.

3.2. Layered Regions

In order to write the approximate wave functions in the layered region $z_q - d/2 < z < z_q + d/2$ $(q = 1, 2, \cdots, Q)$, we measure the position P by means of the local spherical coordinate (r_q, θ_q, ϕ_q) with its origin located at $x = y = 0$ and $z = z_q$. The desired function is

$$\begin{bmatrix} \boldsymbol{E}_N \\ \zeta_0 \boldsymbol{H}_N \end{bmatrix}(P) = \sum_{n=1}^{3N} \sum_{m=-n}^{n} \begin{bmatrix} \boldsymbol{m}_{mn}^{\mathrm{e}}(P) & \boldsymbol{n}_{mn}^{\mathrm{e}}(P) \\ j\boldsymbol{n}_{mn}^{\mathrm{h}}(P) & j\boldsymbol{m}_{mn}^{\mathrm{h}}(P) \end{bmatrix} \begin{bmatrix} C_{mn,N}^{(q)} \\ D_{mn,N}^{(q)} \end{bmatrix} \tag{9}$$

where the vector spherical wave functions are

$$\boldsymbol{m}_{mn}^{\mathrm{e}}(r, \theta, \phi) = \begin{cases} \boldsymbol{\Phi}_{mn}(\hat{J}_n(kr), \theta, \phi) & (r < a) \\ \boldsymbol{\Phi}_{mn}(V_n(k_0 r), \theta, \phi) & (r > a) \end{cases} \tag{10}$$

$$\boldsymbol{n}^{\mathrm{e}}_{mn}(r,\theta,\phi) = \begin{cases} \boldsymbol{\Psi}_{mn}(\hat{J}_n(kr),\theta,\phi) & (r<a) \\ \boldsymbol{\Psi}_{mn}(W_n(k_0 r),\theta,\phi) & (r>a) \end{cases} \tag{11}$$

$$\boldsymbol{m}^{\mathrm{h}}_{mn}(r,\theta,\phi) = \begin{cases} \sqrt{\varepsilon_{\mathrm{r}}}\,\boldsymbol{\Phi}_{mn}(\hat{J}_n(kr),\theta,\phi) & (r<a) \\ \boldsymbol{\Phi}_{mn}(W_n(k_0 r),\theta,\phi) & (r>a) \end{cases} \tag{12}$$

$$\boldsymbol{n}^{\mathrm{h}}_{mn}(r,\theta,\phi) = \begin{cases} \sqrt{\varepsilon_{\mathrm{r}}}\,\boldsymbol{\Psi}_{mn}(\hat{J}_n(kr),\theta,\phi) & (r<a) \\ \boldsymbol{\Psi}_{mn}(V_n(k_0 r),\theta,\phi) & (r>a) \end{cases} \tag{13}$$

with $k = k_0\sqrt{\varepsilon_{\mathrm{r}}}$. These are the solutions of the Helmholtz equation obtained by the method of separation of variables [17]

$$\boldsymbol{\Phi}_{mn}(F(\kappa),\theta,\phi) = \frac{F(\kappa)}{\kappa}\left[-m\,\frac{P_n^{|m|}(\cos\theta)}{\sin\theta}\,\boldsymbol{i}_\theta + j\sin\theta\,P_n^{|m|\prime}(\cos\theta)\,\boldsymbol{i}_\phi\right] \times \mathrm{e}^{jm\phi} \tag{14}$$

$$\boldsymbol{\Psi}_{mn}(F(\kappa),\theta,\phi) = \left\{jn(n+1)\frac{F(\kappa)}{\kappa^2}\,P_n^{|m|}(\cos\theta)\,\boldsymbol{i}_r - \frac{F'(\kappa)}{\kappa} \times \left[j\sin\theta\,P_n^{|m|\prime}(\cos\theta)\,\boldsymbol{i}_\theta + m\,\frac{P_n^{|m|}(\cos\theta)}{\sin\theta}\,\boldsymbol{i}_\phi\right]\right\}\mathrm{e}^{jm\phi} \tag{15}$$

where $P_n^{|m|}$ is the associated Legendre function, and $\hat{J}_n$, V_n, and W_n are the spherical Bessel function [18] and its combinations. See Appendix A for the definition. The prime denotes differentiation with respect to the variable.

We can easily verify that Eq. (9) has already satisfied the boundary conditions on the spherical surfaces

$$\begin{cases} \boldsymbol{i}_{r_q} \times \boldsymbol{E}_N|_{r_q=a+0} = \boldsymbol{i}_{r_q} \times \boldsymbol{E}_N|_{r_q=a-0} \\ \boldsymbol{i}_{r_q} \times \boldsymbol{H}_N|_{r_q=a+0} = \boldsymbol{i}_{r_q} \times \boldsymbol{H}_N|_{r_q=a-0} \end{cases} \tag{16}$$

together with Eqs. (10)–(15) and Appendix A. Equation (9) includes $6QN(3N+2)$ unknown coefficients which depend on the number N. The first finite sum in Eq. (9) is truncated at $n = 3N$ so that the number of unknowns per one layer, $6N(3N+2)$, amounts to about two times as the number of unknowns in each half space, $2(2N+1)^2$. This is because both up- and down-going waves exist in the layered regions.

Figure 2 is a diagram of classifying the expansion coefficients. This provides us intuitive insight into the scattering process as $[\text{incidence}, B] \leftrightarrow [C^{(1)}, D^{(1)}] \leftrightarrow [C^{(2)}, D^{(2)}] \leftrightarrow \cdots \leftrightarrow [C^{(Q)}, D^{(Q)}] \leftrightarrow [A]$. This mechanism makes the matrix block diagonal, which is suitable for effective treatment as will be seen in Section 5.

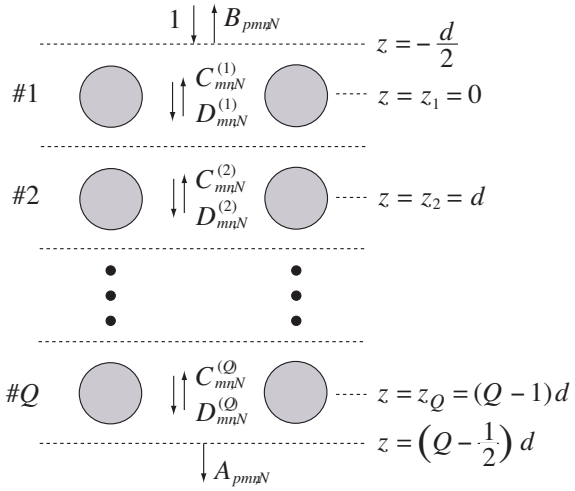

Figure 2. Classification of expansion coefficients.

4. BOUNDARY MATCHING

The continuity of the tangential field components on the planes $z = z_q$ and $x,\ y = \pm d/2$ is given by

$$\left.\begin{aligned} \boldsymbol{i}_z \times (\boldsymbol{E}^{\mathrm{i}} + \boldsymbol{E}_N)|_{z=-d/2-0} &= \boldsymbol{i}_z \times \boldsymbol{E}_N|_{z=-d/2+0} \\ \boldsymbol{i}_z \times (\boldsymbol{H}^{\mathrm{i}} + \boldsymbol{H}_N)|_{z=-d/2-0} &= \boldsymbol{i}_z \times \boldsymbol{H}_N|_{z=-d/2+0} \end{aligned}\right\} \quad (|x| < d/2,\ |y| < d/2) \tag{17}$$

$$\left.\begin{aligned} \boldsymbol{i}_z \times \boldsymbol{E}_N|_{z=z_q+d/2+0} &= \boldsymbol{i}_z \times \boldsymbol{E}_N|_{z=z_q+d/2-0} \\ \boldsymbol{i}_z \times \boldsymbol{H}_N|_{z=z_q+d/2+0} &= \boldsymbol{i}_z \times \boldsymbol{H}_N|_{z=z_q+d/2-0} \end{aligned}\right\} \quad (|x| < d/2,\ |y| < d/2;\ q = 1, 2, \cdots, Q) \tag{18}$$

$$\left.\begin{aligned} \boldsymbol{i}_x \times \boldsymbol{E}_N|_{x=d/2-0} &= \alpha\, \boldsymbol{i}_x \times \boldsymbol{E}_N|_{x=-d/2+0} \\ \boldsymbol{i}_x \times \boldsymbol{H}_N|_{x=d/2-0} &= \alpha\, \boldsymbol{i}_x \times \boldsymbol{H}_N|_{x=-d/2+0} \end{aligned}\right\} \quad (|y| < d/2,\ |z - z_q| < d/2;\ q = 1, 2, \cdots, Q) \tag{19}$$

$$\left.\begin{aligned} \boldsymbol{i}_y \times \boldsymbol{E}_N|_{y=d/2-0} &= \beta\, \boldsymbol{i}_y \times \boldsymbol{E}_N|_{y=-d/2+0} \\ \boldsymbol{i}_y \times \boldsymbol{H}_N|_{y=d/2-0} &= \beta\, \boldsymbol{i}_y \times \boldsymbol{H}_N|_{y=-d/2+0} \end{aligned}\right\} \quad (|x| < d/2,\ |z - z_q| < d/2;\ q = 1, 2, \cdots, Q) \tag{20}$$

The periodicity is incorporated in Eqs. (19) and (20) by means of $\alpha = \mathrm{e}^{-j\alpha_0 d}$ and $\beta = \mathrm{e}^{-j\beta_0 d}$.

Let us distribute the matching points on the square boundary surfaces uniformly as

$$(x,y,z) = \begin{cases} (\xi_i,\ \xi_l,\ -d/2) & \rightarrow \text{ Eq. (17)} \\ (\xi_i,\ \xi_l,\ z_q + d/2) & \rightarrow \text{ Eq. (18)} \\ (\pm d/2,\ \xi_i,\ z_q + \xi_l) & \rightarrow \text{ Eq. (19)} \\ (\xi_i,\ \pm d/2,\ z_q + \xi_l) & \rightarrow \text{ Eq. (20)} \end{cases}$$
$$(i,l = 1,2,\cdots,I;\ q = 1,2,\cdots,Q) \tag{21}$$

with $\xi_i = (2i - 1 - I)d/(2I)$. Imposing Eqs. (17)–(20) at these points, we are led to the set of $4(3Q+1)I^2$ algebraic linear equations for the expansion coefficients. This number of equations stems from the fact that Eq. (21) presents $(3Q+1)I^2$ points or pairs of points, each of which concerns four tangential field components.

The set of linear equations is solved in the sense of least squares [13], where the number I is chosen such that the number of equations is more than that of unknowns. Here, it is effective to use the technique of orthogonal decomposition such as the QR method [16].

5. SEQUENTIAL ACCUMULATIONS (SA)

5.1. Form of Linear Equations

The set of equations under consideration is arranged in the form

$$V\boldsymbol{x} = \boldsymbol{y} \tag{22}$$

which includes the block diagonal matrix of the type

$$V = \begin{bmatrix} V_{11} & V_{12} & 0 & \cdots & 0 & 0 \\ 0 & V_{22} & V_{23} & \cdots & 0 & 0 \\ \vdots & \ddots & \ddots & \ddots & \ddots & \vdots \\ 0 & 0 & 0 & \cdots & V_{KK} & V_{K,K+1} \end{bmatrix} \tag{23}$$

with $K = Q + 1$, as well as the column vectors

$$\boldsymbol{x} = [\boldsymbol{x}_1\ \ \boldsymbol{x}_2\ \ \cdots\ \ \boldsymbol{x}_{K+1}]^{\mathrm{t}}, \quad \boldsymbol{y} = [\boldsymbol{y}_1\ \ \boldsymbol{y}_2\ \ \cdots\ \ \boldsymbol{y}_K]^{\mathrm{t}} \tag{24}$$

The submatrices V_{ij} are constructed from boundary values of the functions $\boldsymbol{e}^{(\pm)}_{pmn} f^{(\pm)}_{mn}$, $\boldsymbol{h}^{(\pm)}_{pmn} f^{(\pm)}_{mn}$, $\boldsymbol{m}^{\mathrm{e}}_{mn}$, and $\boldsymbol{n}^{\mathrm{e}}_{mn}$. The unknown

subvectors $\boldsymbol{x}_k$ are defined by

$$\boldsymbol{x}_k = \begin{cases} [B_{pmn,N}] & (k=1) \\ \begin{bmatrix} C_{mn,N}^{(k-1)} \\ D_{mn,N}^{(k-1)} \end{bmatrix} & (k=2,3,\cdots,Q+1) \\ [A_{pmn,N}] & (k=Q+2) \end{cases} \tag{25}$$

The subvector $\boldsymbol{y}_1$ originates from the incident field in the left hand side of Eq. (17), whereas the other subvectors $\boldsymbol{y}_k$ $(k=2,3,\cdots,K)$ are zero vectors since Eqs. (18)–(20) do not include the incident field.

Let us suppose that V_{ij} is composed of M_i rows and N_j columns. By counting the number of points and elements in Eqs. (21) and (25), respectively, we obtain

$$M_k = \begin{cases} 4I^2 & (k=1) \\ 12I^2 & (k=2,3,\cdots,Q+1) \end{cases} \tag{26}$$

$$N_k = \begin{cases} 2(2N+1)^2 & (k=1,Q+2) \\ 6N(3N+2) & (k=2,3,\cdots,Q+1) \end{cases} \tag{27}$$

5.2. Procedure of SA

Equation (22) is solved by using the technique of sequential accumulation [15] as follows.

SA1 Consider the initial set of Eq. (22), i.e., $[V_{11}\ \ V_{12}][\boldsymbol{x}_1\ \ \boldsymbol{x}_1]^{\mathrm{t}} = \boldsymbol{y}_1$. The QR decomposition $[V_{11}\ \ V_{12}] = Q_1 R_1$ gives that $R_1[\boldsymbol{x}_1\ \ \boldsymbol{x}_1]^{\mathrm{t}} = Q_1^* \boldsymbol{y}_1$, where the matrices Q_1, Q_1^*, and R_1 are unitary, its inverse (conjugate transpose), and upper triangular, respectively. The result is written in the form

$$\begin{bmatrix} R_{11} & R_{12} \\ 0 & \tilde{R}_{22} \end{bmatrix} \begin{bmatrix} \boldsymbol{x}_1 \\ \boldsymbol{x}_2 \end{bmatrix} = \begin{bmatrix} \boldsymbol{z}_1 \\ \tilde{\boldsymbol{z}}_2 \end{bmatrix} \tag{28}$$

where R_{11} and $\tilde{R}_{22}$ are upper triangular.

SA2 We append the latter set of Eq. (28), $\tilde{R}_{22}\boldsymbol{x}_2 = \tilde{\boldsymbol{z}}_2$, to the succeeding set of Eq. (22), $[V_{22}\ \ V_{23}][\boldsymbol{x}_2\ \ \boldsymbol{x}_3]^{\mathrm{t}} = \boldsymbol{y}_2$. This yields the accumulated form

$$\begin{bmatrix} \tilde{R}_{22} & 0 \\ V_{22} & V_{23} \end{bmatrix} \begin{bmatrix} \boldsymbol{x}_2 \\ \boldsymbol{x}_3 \end{bmatrix} = \begin{bmatrix} \tilde{\boldsymbol{z}}_2 \\ \boldsymbol{y}_2 \end{bmatrix} \tag{29}$$

Decomposing the leftmost matrix into Q_2R_2, we have $R_2[\boldsymbol{x}_2 \;\; \boldsymbol{x}_3]^{\mathrm{t}} = Q_2^*[\tilde{\boldsymbol{z}}_2 \;\; \boldsymbol{y}_2]^{\mathrm{t}}$. This is written as

$$\begin{bmatrix} R_{22} & R_{23} \\ 0 & \tilde{R}_{33} \end{bmatrix} \begin{bmatrix} \boldsymbol{x}_2 \\ \boldsymbol{x}_3 \end{bmatrix} = \begin{bmatrix} \boldsymbol{z}_2 \\ \tilde{\boldsymbol{z}}_3 \end{bmatrix} \tag{30}$$

SA3 Sequentially for $k = 3, 4, \cdots, K$, we apply similar manipulations to

$$\begin{bmatrix} \tilde{R}_{kk} & 0 \\ V_{kk} & V_{k,k+1} \end{bmatrix} \begin{bmatrix} \boldsymbol{x}_k \\ \boldsymbol{x}_{k+1} \end{bmatrix} = \begin{bmatrix} \tilde{\boldsymbol{z}}_k \\ \boldsymbol{y}_k \end{bmatrix} \tag{31}$$

This leads to

$$\begin{bmatrix} R_{kk} & R_{k,k+1} \\ 0 & \tilde{R}_{k+1,k+1} \end{bmatrix} \begin{bmatrix} \boldsymbol{x}_k \\ \boldsymbol{x}_{k+1} \end{bmatrix} = \begin{bmatrix} \boldsymbol{z}_k \\ \tilde{\boldsymbol{z}}_{k+1} \end{bmatrix} \tag{32}$$

Only at the final step $k = K$, we will remove the tilde in Eq. (32) like $R_{K+1,K+1}$ and $\boldsymbol{z}_{K+1}$.

SA4 The matrices and vectors without tilde in Eqs. (28), (30), and (32) are extracted and arranged as

$$\begin{bmatrix} R_{11} & R_{12} & 0 & \cdots & 0 & 0 \\ 0 & R_{22} & R_{23} & \cdots & 0 & 0 \\ \vdots & \vdots & \vdots & \ddots & \vdots & \vdots \\ 0 & 0 & 0 & \cdots & R_{KK} & R_{K,K+1} \\ 0 & 0 & 0 & \cdots & 0 & R_{K+1,K+1} \end{bmatrix} \begin{bmatrix} \boldsymbol{x}_1 \\ \boldsymbol{x}_2 \\ \vdots \\ \boldsymbol{x}_K \\ \boldsymbol{x}_{K+1} \end{bmatrix} = [\boldsymbol{z}_1 \;\; \boldsymbol{z}_2 \;\; \cdots \;\; \boldsymbol{z}_K \;\; \boldsymbol{z}_{K+1}]^{\mathrm{t}} \tag{33}$$

This is solved by applying the backward substitution to $R_{K+1,K+1}\boldsymbol{x}_{K+1} = \boldsymbol{z}_{K+1}$ and $R_{kk}\boldsymbol{x}_k = \boldsymbol{z}_k - R_{k,k+1}\boldsymbol{x}_{k+1}$ $(k = K, K-1, \cdots, 2, 1)$.

5.3. Estimation of Computation Time and Memory Requirement

In least squares procedures, the computation time is mainly consumed in QR decompositions. The number of multiplication and division operations included in decomposing one matrix with $\hat{M}$ rows and $\hat{N}$ columns is $\hat{M}(\hat{N}^2+5\hat{N})/2$. This suggests that we may use the function

$$f_\tau(\hat{M}, \hat{N}) = \tau \hat{M} \hat{N}^2 \tag{34}$$

in order to estimate the computation time, where τ is a constant depending on the ability of computer.

If SA is not used, the matrix V in Eq. (23) is decomposed once. In this case the computation time is estimated by

$$\begin{aligned} T &= f_\tau(4(3Q+1)I^2, 4(2N+1)^2 + 6QN(3N+2)) \\ &\approx \tau(3888Q^3 + 8208Q^2 + 5376Q)I^2N^4 \end{aligned} \tag{35}$$

if $N \gg 1$. A similar estimation as SA is employed gives

$$\begin{aligned} T_{\mathrm{SA}} &= \tau f_\tau(M_1, N_1 + N_2) + \tau \sum_{k=2}^{K} f_\tau(N_k + M_k, N_k + N_{k+1}) \\ &\approx \tau(15552Q - 4376)I^2N^4 \end{aligned} \tag{36}$$

with the aid of Eqs. (26) and (27) and the condition $I^2 \gg N^2$. The above two equations lead us to the reduction rate of CPU time as

$$T_{\mathrm{SA}}/T \approx (4Q-1)/[Q(Q+1)^2] \tag{37}$$

Figure 3 is presented to validate the estimation above. The parameters for grating structure do not affect the result and are not filled in. Equations (35) and (36) show that the computational effort for large Q is $O(Q^3)$ and $O(Q^1)$ in the cases without SA and with SA, respectively. The plotted result explains this: the triangular and circular marks are collocated asymptotically along the straight lines of slope 3 and 1. The reduction rate given by Eq. (37) is 0.75, 0.11, and 0.03 for $Q = 1$, 5, and, 10, respectively. Figure 3 obeys these values

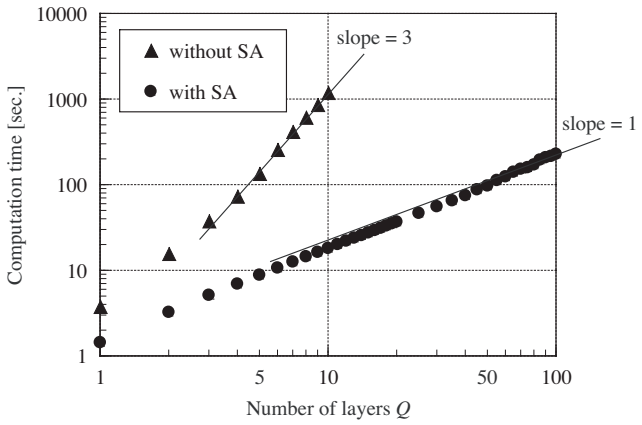

Figure 3. Computation time per one point at $N = 3$ and $I = 10$. A Pentium 4 processor with a clock frequency of 3.0 GHz is used.

relatively well. Therefore we can conclude that the efficacy of SA becomes prominent especially when the number of layer is increased.

In the same manner, the memory is consumed mainly by the matrix V in Eq. (23). To estimate the required memory space S and S_{SA} in the cases without and with SA, respectively, we use the function

$$g_\sigma(\hat{M}, \hat{N}) = \sigma \hat{M} \hat{N} \tag{38}$$

where σ is a constant. Replacement of f_r by g_σ in Eqs. (35) and (36) yields $S \approx \sigma \cdot 216 Q^2 I^2 N^2 = O(Q^2)$ and $S_{\mathrm{SA}} \approx \sigma \cdot 432 Q I^2 N^2 = Q(Q^1)$, which leads us to

$$S_{\mathrm{SA}}/S \approx 2/Q \tag{39}$$

Therefore we can conclude that SA works well from the viewpoint of both CPU time and memory.

6. NUMERICAL RESULTS

6.1. Convergence

In order to determine the number I for a given N, we utilize the fact that $\hat{M} \geq \hat{N}$ must hold in Eq. (34). This rule is applied to Eq. (36) to yield

$$\begin{cases} M_1 \geq N_1 + N_2 \\ N_k + M_k \geq N_k + N_{k+1} \quad (k = 2, 3, \cdots, K) \end{cases} \tag{40}$$

which is combined with Eq. (26) and (27). We select the minimum even number I as shown in Table 1.

Table 1. Determination of the number of matching points.

N	1	2	3	4	5	6	7	8	9	10
I	4	8	10	12	14	18	20	22	24	28

In order to discuss the convergence of the numerical solution, we define the normalized mean square error by

$$\Omega_N^{\mathrm{ms}} = ||V\boldsymbol{x} - \boldsymbol{y}||^2 / ||\boldsymbol{y}||^2 \tag{41}$$

where $\boldsymbol{x}$ is a solution of Eq. (33), and $||*||$ denotes a magnitude of column vector. As another check of the accuracy, we define the energy error by

$$\Omega_N^{\mathrm{en}} = 1 - \sum_{p=1}^{2} \sum_{\substack{m,n \\ (\mathrm{Re}\,\gamma_{mn} > 0)}} (P_{pmn}^{\mathrm{t}} + P_{pmn}^{\mathrm{r}}) \tag{42}$$

where the second sum in Eq. (42) covers only propagating modes, and the normalized transmitted and reflected powers are computed by

$$\begin{cases} P^{\mathrm{t}}_{pmn} = \mathrm{Re}\,(\gamma_{mn}/\gamma_{00})\,|A_{pmn,N}|^2 \\ P^{\mathrm{r}}_{pmn} = \mathrm{Re}\,(\gamma_{mn}/\gamma_{00})\,|B_{pmn,N}|^2 \end{cases} \tag{43}$$

As shown in Fig. 4, both of the errors decrease monotonically when N increases. Since the wavelength in the dielectric is shorter than that in the air, we need large N for big spheres. However, even for $a/d = 0.4$, these errors become less than 1% if $N \geq 5$. The computations hereafter will be performed under the conditions that the errors are usually below 0.1%, but we permit 1%-error only in rapidly changing portions of curves.

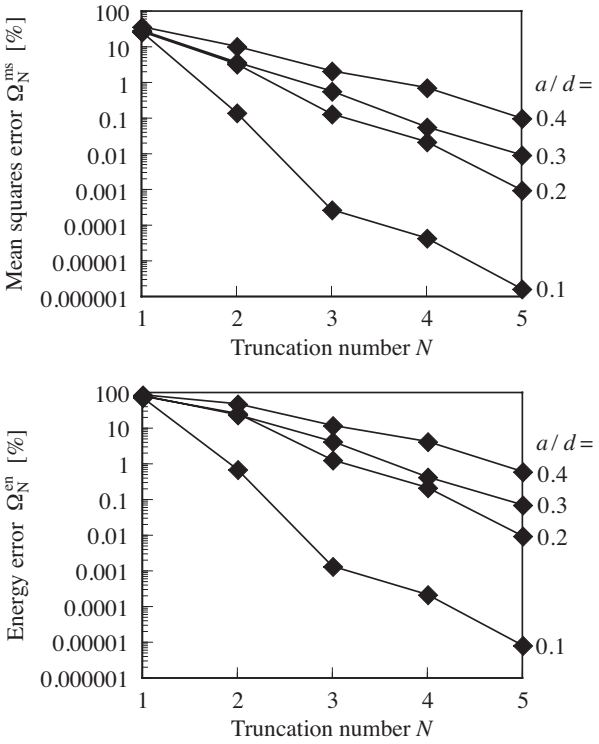

Figure 4. Mean squares error and energy error at $Q = 2$, $\varepsilon_{\mathrm{r}} = 10$, $d/\lambda = 0.8$, and $\theta^{\mathrm{i}} = \phi^{\mathrm{i}} = \delta = 0^\circ$.

6.2. Physical Properties

Figure 5 shows the transmitted powers for single layered arrays in the single mode region at normal incidence, where the result is independent of polarization. We fix the parameters a/d and ε_{r} in Figs. 5(a) and 6(b), respectively. The solid line in Fig. 5(b) is terminated at $d/\lambda = 0.63$, since at higher frequencies the curve would change rapidly and disturb

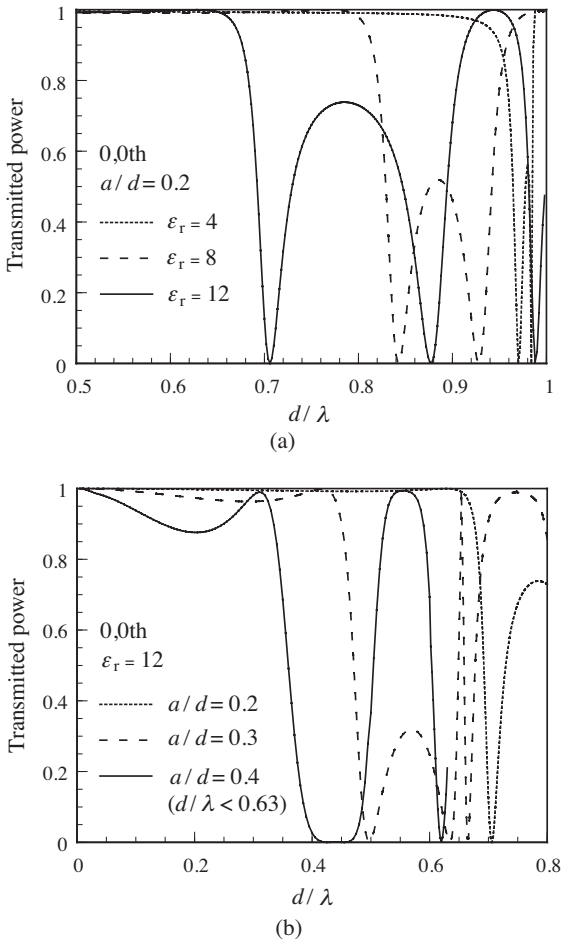

Figure 5. Frequency characteristics of transmitted powers of the dominant mode for single layered arrays ($Q = 1$) at normal incidence ($\theta^{\mathrm{i}} = \phi^{\mathrm{i}} = 0°$), with δ being arbitrary.

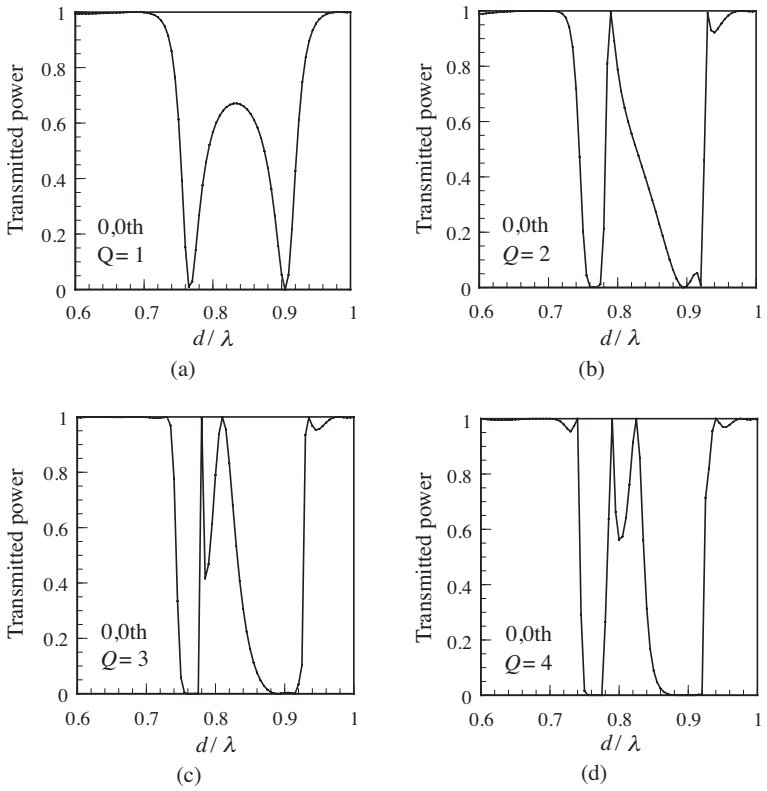

Figure 6. Frequency characteristics of transmitted powers of the dominant mode for four different numbers of layers at normal incidence. The parameters are $a/d = 0.2$, $\varepsilon_{\mathrm{r}} = 10$, and $\theta^{\mathrm{i}} = \phi^{\mathrm{i}} = 0^{\circ}$, with δ being arbitrary.

the sight of other curves. Generally speaking, when ε_{r} or a/d is increased, the transmission band becomes narrow and the points of total reflection shift toward the low frequency side. We also find it difficult to widen the total reflection region by using single layers of small spheres.

Figure 6 is drawn to observe the effect of increasing the layer number on the band of total transmission/reflection. The behavior of Fig. 6(a) for single layer is the middle between the solid and dotted curves in Fig. 5(a): we have total reflection points at $d/\lambda \approx 0.77$ and 0.91. When the layer is increased, these points are gradually changed to reflection bands having some width, and a new reflection band is under formation between these bands, i.e., $0.78 < d/\lambda < 0.84$.

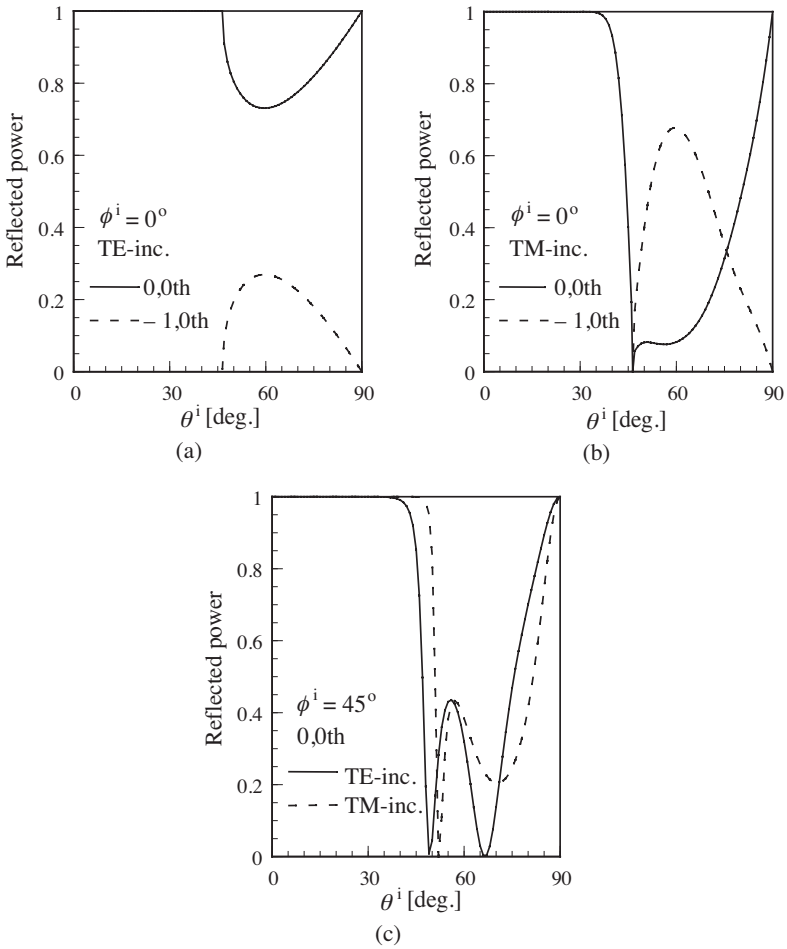

Figure 7. Dependence of reflected powers on the incident angles. The parameters are $Q = 4$, $a/d = 0.25$, $\varepsilon_r = 12$, and $d/\lambda = 0.58$.

Figure 7 presents the reflected power for each mode as a function of incident angle θ^i. Another incident angle ϕ^i is fixed at two typical values, 0° and 45° for Fig. 7(a)(b) and (c), respectively. We observe the total reflection when θ^i is less than about 40°. This property disappears for larger θ^i due to the emergence of higher order modes. In general, achievement of perfect band gap requires special technique in designing grating structures [6, 7].

7. CONCLUSIONS

We have presented the method of solution to the electromagnetic scattering from multilayered periodic arrays of dielectric spheres. Detailed descriptions were given for the approximate mode functions, boundary matching, and sequential accumulation (SA) procedure. We discussed the convergence of solutions and some band gap characteristics, and verified the efficacy of introducing SA.

The present approach is also applicable to wide range of scattering problems having cascaded boundary structures. To name a few, band gap materials by stratified dielectric rods, metallic waveguide filters, and dielectric bodies of revolution belong to this category. These deserve further attention.

ACKNOWLEDGMENT

The authors thank Mr. M. Satoh, previous graduate student of Kumamoto University and presently a member of Hitachi, Ltd., for his assistance in numerical computations.

APPENDIX A. SPHERICAL BESSEL FUNCTIONS

The spherical Bessel functions appearing in Eqs. (10)–(13) are defined by [18]

$$\hat{Z}_n(x) = \sqrt{\frac{\pi x}{2}} Z_{n+1/2}(x) \tag{A1}$$

where Z_ν stands for conventional Bessel functions of the first kind J_ν or the second kind Y_ν. The field outside the spheres is expressed in terms of

$$V_n(x) = \left(\frac{y'_{n0}\, j_n}{\sqrt{\varepsilon_r}} - y_{n0}\, j'_n \right) \hat{J}_n(x) - \left(\frac{j'_{n0}\, j_n}{\sqrt{\varepsilon_r}} - j_{n0}\, j'_n \right) \hat{Y}_n(x) \tag{A2}$$

$$W_n(x) = \left(y'_{n0}\, j_n - \frac{y_{n0}\, j'_n}{\sqrt{\varepsilon_r}} \right) \hat{J}_n(x) - \left(j'_{n0}\, j_n - \frac{j_{n0}\, j'_n}{\sqrt{\varepsilon_r}} \right) \hat{Y}_n(x) \tag{A3}$$

where

$$\begin{cases} j_{n0} = \hat{J}_n(k_0 a), & j'_{n0} = \hat{J}'_n(k_0 a) \\ y_{n0} = \hat{Y}_n(k_0 a), & y'_{n0} = \hat{Y}'_n(k_0 a) \\ j_n = \hat{J}_n(ka), & j'_n = \hat{J}'_n(ka) \end{cases} \tag{A4}$$

The Lommel formula $j_{n0}\, y'_{n0} - j'_{n0}\, y_{n0} = 1$ is used to verify the boundary conditions (16) on the spherical surface.

REFERENCES

1. Venakides, S., M. Haider, and V. Papanicolaou, "Boundary integral calculations of 2-d electromagnetic scattering by photonic crystal Fabry-Perot structures," *SIAM J. Appl. Math.*, Vol. 60, No. 5, 1686–1706, 2000.
2. Yamasaki, T., T. Hinata, and T. Hosono, "Scattering of electromagnetic waves by columnar dielectric gratings with elliptically layered media," *Trans. IEE Japan*, Vol. 122-A, No. 1, 28–33, 2002.
3. Yasumoto, K., H. Toyama, and T. Kushta, "Accurate analysis of two-dimensional electromagnetic scattering from multilayered periodic arrays of circular cylinders using lattice sums technique," *IEEE Trans. Antennas Propagat.*, Vol. AP-52, No. 10, 2603–2611, 2004.
4. Matsushima, A., "Equivalent circuit parameters for gratings composed of dielectric circular cylinders," *IEICE Trans. Electron. (Japanese Edition)*, Vol. J88-C, No. 7, 585–588, 2005.
5. Yablonovitch, E., "Inhibited spontaneous emission in solid-state physics and electronics," *Phys. Rev. Lett.*, Vol. 58, 2059–2062, 1987.
6. Ho, K. M., C. T. Chan, and C. Soukoulis, "Existence of a photonic gap in periodic dielectric structures," *Phys. Rev. Lett.*, Vol. 65, No. 25, 3152–3155, 1990.
7. Li, X.-J., W.-X. Zhang, L.-G. Zheng, and P. Lu, "The stratified dielectric gratings used as 3-D EBG structure," *J. of Electromagn. Waves and Appl.*, Vol. 18, No. 10, 1347–1359, 2004.
8. Fu, Y. and N. Yuan, "Accurate analysis of electromagnetic bandgap materials using moment methods," *J. of Electromagn. Waves and Appl.*, Vol. 19, No. 5, 629–653, 2005.
9. Hattori, H. T., A. Kazmierczak, V. M. Schneider, and C. L. Barbosa, "Photonic crystal micro-cavity based radiation filter," *J. of Electromagn. Waves and Appl.*, Vol. 19, No. 11, 1525–1534, 2005.
10. Boag, A., Y. Leviatan, and A. Boag, "Analysis of electromagnetic scattering from doubly periodic arrays of penetrable bodies using a patch-dipole current model," *Radio Sci.*, Vol. 26, No. 2, 603–610, 1991.
11. Okuno, Y., "The mode-matching method," *Analysis Methods for Electromagnetic Wave Problems*, E. Yamashita (ed.), Ch. 4, Artech House, Boston, 1990.
12. Davies, J. B., "A least-squares boundary residual method in

the numerical solution of scattering problems," *IEEE Trans. Microwave Theory Tech.*, Vol. MTT-21, No. 2, 99–104, 1973.

13. Ikuno, H. and K. Yasuura, "Improved point-matching method with application to scattering from a periodic surface," *IEEE Trans. Antennas Propagat.*, Vol. AP-21, No. 5, 657–662, 1973.
14. Ohtsu, M., Y. Okuno, A. Matsushima, and T. Suyama, "Combination of up- and down-going Floquet modal functions used to describe the field inside grooves of a deep grating," *Progress In Electromagnetics Research*, PIER 64, 293–316, 2006.
15. Lawson, C. L. and R. J. Hanson, *Solving Least Squares Problems*, Ch. 27, SIAM, Philadelphia, PA, 1995.
16. Press, W. H., B. P. Flannery, S. A. Teukolsky, and W. T. Vetterling, "QR decomposition," *Numerical Recipes in FORTRAN 77: The Art of Scientific Computing*, Sec. 2.10, Cambridge University Press, Cambridge, 1992.
17. Stratton, J. A., *Electromagnetic Theory*, Ch. 7, McGraw-Hill, NY, 1941.
18. Schelkunoff, S. A., *Electromagnetic Wave*, Ch. 3, Van Nostrand, NY, 1943.